

ExCALIBUR

Selection of techniques for Model Order Reduction

M2.5.2

The report describes work for ExCALIBUR project NEPTUNE at Milestone 2.5.2. This binds the reports 2047352_2-TN-01[1] and 2047352_2-TN-02[2] as of August 27, 2021, which are presented in composite form: sections 2 and 3 (pp.1-7 of total 20 pp) comprise the original 2047352_2-TN-01.

The aim of this report is to provide a preliminary description of potential reduction of size of inputs, size of design, and size of outputs, and associated computational benefits of reduced order modelling for fusion codes, with a focus on relevant proxyapps. Due to time constraints, a single proxyapp - describing anisotropic heat transport - is considered, though this is supported by toy examples and further references from the oeuvre of the authors (who are world experts in the field), including illustrative examples of coupled models.

The report stresses the need for reduced order models (hereafter ROMs) in situations mandating large ensembles of expensive simulations (as are expected to arise in NEPTUNE for e.g. uncertainty quantification or data assimilation aspects). A bird's eye perspective on the subject area is provided and justification is given for the decisions to focus primarily on non-intrusive ROMs - meaning that there is no need to alter the subject simulation code; the ROM is then 'data-driven' in that it is constructed using solely the outputs of the subject - a decision entirely consistent with the NEPTUNE separation of concerns ethos, and more specifically to use the family of Gaussian process surrogates (hereafter GP-ROM). Some relevant aspects of the current state-of-the-art are indicated, with reference to the authors' recent works.

The report details a particular non-intrusive ROM as applied to the anisotropic diffusion problem (viz. a two-dimensional diffusion equation in which the diffusivity is represented by a spatially-varying anisotropic tensor). The numerical representation is via the finite-element package `Firedrake`, giving a solution comprising 78961 degrees of freedom. This model space dimensionality is reduced to 25 using the technique of proper orthogonal decomposition (POD); the reduced system is then used to fit a Gaussian process using a constant mean (trend function) and a Matérn kernel for the prior covariance. The efficacy of the resulting model, in terms of predicted mean and confidence interval, is shown to be reasonable by comparing some of the ROM outputs to the corresponding full numerical solutions. This section contains also a technical exposition of the offline regression used to construct the Gaussian process, in which the main computational bottleneck - a cubic scaling in the number of data samples - is emphasized.

A subsequent section provides a description of active learning (AL) for constructing a GP-ROM. AL entails choosing the next sampling position dynamically based on the current ROM - various algorithms can be used: the Mackay strategy (giving ALM) is to minimize the local maximum

posterior predictive variance, leading to the problem of over-sampling at boundaries, while the alternate Cohn scheme (ALC) involves minimizing the same variance averaged over the domain (the need for additional model evaluations during these steps is avoided by a property of Gaussians under Bayesian combination). The AL schemes are applied to the anisotropic diffusion problem, demonstrating that (1) the active learning saturates at large sample numbers giving there similar performance to a static Latin hypercube design (LHD); and (2) the ALM performs worse than ALC or a LHD at large sample number because of the boundary over-sampling problem. For realistic fusion problems, the samples are likely to be sufficiently expensive that the saturated regime is not encountered, hence AL is expected to be useful. The authors propose also a strategy for identifying and excluding regions of flat response surface in the offline phase, in order to mitigate against the cubic scaling problem in fitting a GP-ROM with a large number of samples - this involves a dense exploration of the response surface and then the selection from these outputs of an appropriate set of initial data, followed by active learning using the data already generated (thus giving a procedure that is explicitly parallelizable). This approach provides arguably some protection against the problem of missing extreme outlying events - one must bear in mind that the quality of the ROM is to a large extent dependent on the experimental design. As a caution, however, it must be noted that, for the NEPTUNE use case, a dense sampling of the response surface is likely to represent a very large computational challenge.

The report closes with a discussion of possible future directions in a section in which the recommendations interspersed at appropriate locations serve in lieu of a formal concluding section. A proposal to test some intrusive methods in order to mitigate the problem of excluding extreme events when applying dimension reduction techniques (e.g. POD) is included; the output here would be a physics-informed ROM (references in the context of machine learning are given).

A subsection presents deep GPs (meaning that the outputs of a GP are used sequentially as the inputs to another GP) where the motivation is to construct ROMs for systems with regime change; the deep GP is able to incorporate multiple kernels, as evidenced by the example of fitting a toy dataset containing distinct quiescent and active regions.

A further subsection focuses on active subspace methods for reducing the *input* dimension (cf. the POD in Section 3, which reduces the number of internal model states). A technique called *sufficient dimension reduction* is briefly outlined (with further reference provided), giving a general method for detecting the linear combinations of inputs to which a model is most sensitive.

A final subsection outlines, with the aid of a toy example, linked GPs, which differ from deep GPs in that they model a system that can be explicitly decomposed into component parts, the simpler components being more amenable to GP emulation than is the whole (the divide-and-conquer principle applies). This gives also a semi-intrusive procedure for constructing a GP-ROM for a coupled system. It is explained that there remain challenges associated to the dimension reduction of the intermediate data in cases where the intermediate states have input dimension much higher than that of the global input. It is clear that active sampling in the case of a linked GP can mitigate the problem of under-exploration of the input parameter space of intermediate components in a coupled model i.e. the fact that the space-filling property of a LHD is lost once the inputs have been propagated through one or more component models (thus giving, amongst other problems, the potential to miss extreme events).

Acknowledgement

The support of the UK Meteorological Office and Strategic Priorities Fund is acknowledged.

References

- [1] D. Ming and S. Guillas. Report on suitability and potential of ROM to fusion models : A Non-intrusive ROM for Solvers with High-dimensional Outputs. Technical Report 2047352.2-TN-01, UKAEA Project Neptune, 2021.
- [2] D. Ming and S. Guillas. Report on suitability and potential of Reduced Order Modelling (ROM) to fusion models: Gaussian Process ROM for Solvers with High-dimensional Outputs. Technical Report 2047352.2-TN-02, UKAEA Project Neptune, 2021.

UKAEA REFERENCE AND APPROVAL SHEET

	Client Reference:		
	UKAEA Reference:		CD/EXCALIBUR-FMS/0044
	Issue:		1.00
	Date:		August 27, 2021
Project Name: ExCALIBUR Fusion Modelling System			
	Name and Department	Signature	Date
Prepared By:	Wayne Arter Ed Threlfall BD	N/A N/A	August 27, 2021 August 27, 2021
Reviewed By:	Rob Akers Advanced Computing Dept. Manager		August 27, 2021
Approved By:	Martin O'Brien MSSC		August 27, 2021

Report on suitability and potential of Reduced Order Modelling (ROM) to fusion models

Gaussian Process ROM for Solvers with High-dimensional Outputs

Deyu Ming and Serge Guillas

University College London

UKAEA Report: 2047352_2-TN-02 D1.1

Final report

August 2, 2021

1 Disclaimer

We are very grateful to Dr Patrick Farrell for the provision of the proxyApp modelling the anisotropic heat transport problem. It is the only fusion model we could access over the short period of the funded project (4 January 2021 - 31 July 2021). We discussed with the NEPTUNE team (Benjamin Dudson and Patrick Farrell) the possibility of using another model to couple two models in a one-way coupling for UQ using ROM: the anisotropic heat transport model and the isotropic heat conduction to the solid wall. But the wall boundary proxyApp is not yet available. As a result, we could not examine in practice the possibility of implementing ROM for UQ in the context of nuclear fusion modelling where models are coupled. We nevertheless provided some examples of UQ coupling at the end of this report from the paper Ming and Guillas (2021) and discussed future directions below.

2 Introduction

Many modern physical computer models involve solving PDEs with numerical solvers, such as finite element methods (FEM), which can be computationally expensive due to

- ever more complex and larger-scale models;
- high-dimensional input and output;
- large demands on computational resources.

These create challenges to efficient uncertainty quantification of computer models, such as the fusion models, as we often need to run the models many times for tasks such as sensitivity analysis, uncertainty propagation and model calibration. To tackle these challenges, reduced order models (ROM) are needed to

- serve as low-dimensional replacements with comparable accuracy;
- reduce evaluation time of original solvers;
- save storage, e.g., for high-dimensional output.

32 Traditional reduced order models, also known as intrusive reduced order models, often are
33 constructed using reduced basis methods (Quarteroni et al., 2015), among which the Proper
34 Orthogonal Decomposition (POD) is perhaps the most popular technique. The intrusive reduced
35 order models for original high-fidelity models with high-dimensional output are typically built
36 using a two-phase procedure called offline-online decomposition:

- 37 • *offline phase*: high-fidelity solutions/outputs are obtained and reduced basis is calculated;
- 38 • *online phase*: the original problems are projected onto the reduced space for efficient
39 computation of solutions at new inputs.

40 However, the online phase of the intrusive reduced order modelling is challenging in practice
41 because:

- 42 • expertise and domain knowledge are required to project the equations and physics of the
43 original high-fidelity problems to constructed reduced space;
- 44 • dimensionality reduction techniques are largely constrained by the problem formulation;
- 45 • uncertainty is not incorporated.

46 For these reasons, in this report we focus on non-intrusive reduced order models for problems
47 with high dimensional outputs, utilising the family of Gaussian process (GP) surrogates (also
48 known as emulators). GP emulators have been successfully implemented for dimension reduction
49 of either outputs or inputs. For instance:

- 50 • Guillas et al. (2018) used Functional Principal Components Analysis (FPCA) as an equiv-
51 alent approach to POD for time series outputs of tsunami waves, and Chang et al. (2019)
52 used Spherical Harmonics and Gaussian Markov Random Fields for optimal reduction of
53 surfaces outputs.
- 54 • For inputs, Liu and Guillas (2017) employed a kernel-based approach to extract the few
55 input field directions of most influence for the outputs in order to build GPs with few
56 input dimensions (orders of magnitude gain in dimension).

57 The report is organised as follows. In Section 3, a non-intrusive ROM with GP surrogates
58 and POD is described and applied in a anisotropic heat transport problem. We then propose
59 and discuss an active learning procedure to construct the introduced non-intrusive ROM with
60 an illustrative example in Section 4. Future directions are discussed in Section 5.

61 **3 Non-intrusive ROM with Gaussian Process Surrogates**

62 The non-intrusive reduced order modelling is a data-driven approach that uses a statistical
63 surrogate model to mimic the functional relations between the model input and constructed
64 reduced output space in the online phase of the offline-online decomposition. The utilisation of
65 statistical surrogates alleviates the difficulties involved in reformulating the original high-fidelity
66 problems under the intrusive reduced order modelling. In particular, with GP surrogates we

67 are able to quantify uncertainty of the high-dimensional outputs predicted at unobserved input
 68 positions.

69 Let $\mathbf{X} \in \mathbb{R}^{N \times D}$ contain N sets of D dimensional input of a computer model, which produces
 70 N corresponding sets of K dimensional output $\mathbf{Y} \in \mathbb{R}^{N \times K}$ accordingly. Then, one can mimic
 71 the functional relationships between the input \mathbf{X} and each output dimension $\mathbf{Y}_k \in \mathbb{R}^{N \times 1}$ by a
 72 GP surrogate \mathcal{GP}_k independently for $k = 1, \dots, K$ without considering the dependence between
 73 output dimensions (Gu and Berger, 2016). Ignoring the potential cross-dependence does not
 74 pose a serious issue unless we are interested in the joint distribution of the output, and it can be
 75 shown (Kzyurova, 2017) that the independently constructed GP surrogates correspond to the
 76 marginal GPs of a joint GP surrogate under certain dependence structures. The GP surrogate
 77 \mathcal{GP}_k is formally defined as a multivariate normal distribution with respect to \mathbf{Y}_k :

$$78 \quad \mathbf{Y}_k \sim \mathcal{N}(\boldsymbol{\mu}_k(\mathbf{X}), \sigma_k^2 \mathbf{R}_k(\mathbf{X})),$$

79 in which the i -th element of $\boldsymbol{\mu}_k(\mathbf{X}) \in \mathbb{R}^{N \times 1}$ is often specified by a trend function $f_k(\mathbf{X}_i)$ with
 80 $\mathbf{X}_i \in \mathbb{R}^{1 \times D}$ being the i -th row of \mathbf{X} , and the ij -th element of $\mathbf{R}_k(\mathbf{X}) \in \mathbb{R}^{N \times N}$ is given by
 81 $c_k(\mathbf{X}_i, \mathbf{X}_j)$, where c_k is a given kernel function. The trend function f_k can be formulated as a
 82 linear combination of a set of basis functions of \mathbf{X}_i and we assume a constant trend function
 83 $f_k(\mathbf{X}_i) = b_k$ in this report.

84 There are various choices for c_k (see Rasmussen and Williams (2006)). In this report, we use
 85 the separable kernel function:

$$86 \quad c_k(\mathbf{X}_i, \mathbf{X}_j) = \prod_{d=1}^D c_{k,d}(X_{id}, X_{jd}),$$

87 where $c_{k,d}$ is a one-dimensional kernel function. A typical choice for $c_{k,d}$ in computer model
 88 emulation is the squared exponential (SExp) kernel:

$$89 \quad c_{k,d}(X_{id}, X_{jd}) = \exp \left\{ -\frac{(X_{id} - X_{jd})^2}{\gamma_{k,d}^2} \right\},$$

90 where $\gamma_{k,d} > 0$ is the range parameter. However, the SExp kernel has been criticised for its
 91 over-smoothness (Stein, 1999) for physical problems as well as its associated ill-conditioned
 92 problems (Dalbey, 2013; Gu et al., 2018b). Another popular kernel choice is the Matérn ker-
 93 nel (Rasmussen and Williams, 2006):

$$94 \quad c_{k,d}(X_{id}, X_{jd}) = \exp \left(-\frac{\sqrt{2p+1} r_{ij,d}}{\gamma_{k,d}} \right) \frac{p!}{(2p)!} \sum_{i=0}^p \frac{(p+i)!}{i!(p-i)!} \left(\frac{2r_{ij,d}\sqrt{2p+1}}{\gamma_{k,d}} \right)^{p-i},$$

95 where $r_{ij,d} = |X_{id} - X_{jd}|$. The Matérn kernel is known to be less prone to ill-conditioning
 96 issues and provides a reasonably adequate smoothness to the GP surrogates. In particular, the
 97 Matérn-2.5 kernel, which is defined as the Matérn kernel with $p = 2$:

$$98 \quad c_{k,d}(X_{id}, X_{jd}) = \left(1 + \frac{\sqrt{5}|X_{id} - X_{jd}|}{\gamma_{k,d}} + \frac{5(X_{id} - X_{jd})^2}{3\gamma_{k,d}^2} \right) \exp \left\{ -\frac{\sqrt{5}|X_{id} - X_{jd}|}{\gamma_{k,d}} \right\},$$

99 is the default kernel choice for many computer model emulation packages, such as `DiceKriging` (Rous-
 100 tant et al., 2012) and `RobustGaSP` (Gu et al., 2018a). Therefore, we employ the Matérn-2.5 kernel
 101 in this report.

102 The posterior predictive distribution $\mathcal{N}(\hat{\mu}_k(\mathbf{x}^*), \hat{\sigma}_k^2(\mathbf{x}^*))$ of \mathcal{GP}_k with respect to the output
 103 $Y_k^*(\mathbf{x}^*)$ at an unobserved input position \mathbf{x}^* is given in different analytical forms depending
 104 on how the model parameters b_k , σ_k^2 and $\{\gamma_{k,d}\}_{d=1,\dots,D}$ are estimated. Different maximum-
 105 likelihood-based estimation approaches and the corresponding expressions for $\hat{\mu}_k(\mathbf{x}^*)$ and $\hat{\sigma}_k^2(\mathbf{x}^*)$
 106 are discussed in Roustant et al. (2012); Gu et al. (2018b).

107 The main computational bottlenecks of the GP surrogate construction are the number of
 108 data points N and the dimension K of the output of a computer model. Since the inference
 109 of GP surrogates involve inversions of the correlation matrix $\mathbf{R}_k \in \mathbb{R}^{N \times N}$ with computational
 110 complexity of $\mathcal{O}(N^3)$, it soon becomes computationally prohibitive to build GP surrogates in
 111 practice when N is more than several thousands. In such a case, one may need sparse approx-
 112 imations (Liu et al., 2020) to the GP to reduce the computational complexity induced by the
 113 big data.

114 In computer model experiments, one often does not have big data (i.e., realisations from
 115 the underlying computer model) due to the limited computational budget. However, if the
 116 input dimension D is large, then small data are insufficient to explore adequately the whole
 117 input domain and thus the resulting GP surrogates can be inaccurate. High input dimension
 118 also causes challenges to the model estimation because a large number of range parameters
 119 $\{\gamma_{k,d}\}_{d=1,\dots,D}$ need to be estimated for each output dimension. To alleviate this issue, one can
 120 reduce the input dimension D to P such that $P \ll D$ by dimension reduction techniques such as
 121 POD, kernel dimension reduction (Liu and Guillas, 2017), and active subspace (Tripathy et al.,
 122 2016).

123 A high output dimension K creates the issue that it can be computational burdensome to
 124 build K independent GP surrogates: without parallel implementation the training and validation
 125 of a huge amount of GP surrogates are practically infeasible. This report tackles the latter issue
 126 on high-dimensional outputs (e.g., a snapshot where each point on the snapshot represents a FE
 127 solution and contributes to the output dimensionality) produced by computer models. Perhaps
 128 the most straightforward approach to address the issue is to reduce the output dimension K to
 129 L such that $L \ll K$ by POD.

130 The POD of $\mathbf{Y} \in \mathbb{R}^{N \times K}$ can be done with following steps:

- 131 1. Compute the sample mean $\boldsymbol{\mu}_{\mathbf{Y}} \in \mathbb{R}^{1 \times K}$ of \mathbf{Y} and obtain the centred output matrix $\mathbf{Y}_c =$
 132 $\mathbf{Y} - \boldsymbol{\mu}_{\mathbf{Y}}$;
- 133 2. Implement the eigendecomposition of $\mathbf{G} = \frac{1}{N} \mathbf{Y}_c \mathbf{Y}_c^\top$ such that $\mathbf{G} = \mathbf{V} \boldsymbol{\Lambda} \mathbf{V}^\top$, where the
 134 columns of $\mathbf{V} \in \mathbb{R}^{N \times N}$ contains the eigenvectors of \mathbf{G} and the diagonal of $\boldsymbol{\Lambda} \in \mathbb{R}^{N \times N}$
 135 contains the corresponding eigenvalues $(\lambda_1, \dots, \lambda_N)$ in descending order;
- 136 3. Compute $\tilde{\mathbf{V}} = \mathbf{Y}_c^\top \mathbf{V} \in \mathbb{R}^{K \times N}$, which contains the eigenvectors of sample covariance matrix
 137 $\mathbf{C} = \frac{1}{N} \mathbf{Y}_c^\top \mathbf{Y}_c$;
- 138 4. Choose $L \leq N$ and obtain the low dimensional output $\hat{\mathbf{Y}} = \mathbf{Y}_c \tilde{\mathbf{V}}_L \in \mathbb{R}^{N \times L}$, where

139 $\tilde{\mathbf{V}}_L \in \mathbb{R}^{K \times L}$ contains the first L eigenvectors included in $\tilde{\mathbf{V}}$.

140 One can also obtain $\tilde{\mathbf{V}}$ by performing the singular value decomposition (SVD) of \mathbf{Y}_c that is im-
 141 plemented, e.g., in the PCA function of Python package `scikit-learn` (Pedregosa et al., 2011).
 142 After obtaining the low dimensional data $\hat{\mathbf{Y}}$, we then construct L independent GP surrogates
 143 of each of L dimensions of $\hat{\mathbf{Y}}$. Let $\mathcal{N}(\hat{\mu}_l(\mathbf{x}^*), \hat{\sigma}_l^2(\mathbf{x}^*))$ be the posterior predictive distribution
 144 of $\hat{Y}_l^*(\mathbf{x}^*)$, the l -th dimension of the low dimensional output, predicted at an unobserved input
 145 position \mathbf{x}^* . Then the posterior predictive distribution of the corresponding high dimensional
 146 output $\mathbf{Y}^*(\mathbf{x}^*) \in \mathbb{R}^{1 \times K}$ is given by

$$147 \quad \mathcal{N}\left(\hat{\boldsymbol{\mu}}(\mathbf{x}^*)\tilde{\mathbf{V}}_L^\top + \boldsymbol{\mu}_{\mathbf{Y}}, \tilde{\mathbf{V}}_L\hat{\boldsymbol{\Sigma}}(\mathbf{x}^*)\tilde{\mathbf{V}}_L^\top\right),$$

148 where $\hat{\boldsymbol{\mu}}(\mathbf{x}^*) = (\hat{\mu}_1(\mathbf{x}^*), \dots, \hat{\mu}_L(\mathbf{x}^*))$ and $\hat{\boldsymbol{\Sigma}}(\mathbf{x}^*) = \text{diag}(\hat{\sigma}_1^2(\mathbf{x}^*), \dots, \hat{\sigma}_L^2(\mathbf{x}^*))$.

149 Figure 1 demonstrates the procedure to build non-intrusive reduced order model with GP
 150 surrogates. In the offline phase, dimension-reduction techniques, e.g., POD, are applied to
 151 reduce the high-dimensional output to a low-dimensional space. Then in the online phase, GP
 152 surrogates are constructed independently on each reduced dimension. Using the constructed
 153 GP surrogate and reduced basis, one can obtain the predicted low-dimensional and in turn the
 154 high-dimensional output at new input positions with little computational efforts.

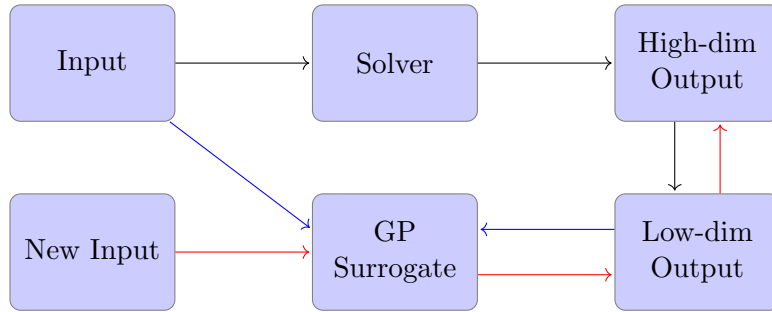


Figure 1: The workflow to construct non-intrusive ROM with GP. The black arrows represent the offline phase; the blue arrows represent the online phase; the red arrows represent the prediction procedure using the constructed non-intrusive ROM with GP.

155 3.1 Example: 2-D model of anisotropic heat transport

156 In this section, we explore the non-intrusive ROM with GP to mimic the FE solver to the 2-D
 157 problem “Open field lines with oscillating anisotropy directions” in Deluzet and Narski (2019).
 158 The problem has two key inputs m and α that control the anisotropy of the solution field, i.e.,
 159 the anisotropy direction is defined by

$$160 \quad \mathbf{b} = \frac{\mathbf{B}}{|\mathbf{B}|}, \quad \mathbf{B} = \begin{pmatrix} \alpha(2y - 1) \cos(m\pi x) + \pi \\ \pi\alpha m(y^2 - y) \sin(m\pi x) \end{pmatrix},$$

161 where $m/2$ is the number of oscillation periods in the computational domain and α is the
 162 amplitude. The output is a high-dimensional 2-D field defined on the square computational
 163 domain $[0, 1] \times [0, 1]$ and allows a closed form solution.

164 3.1.1 Experimental Setup

165 To construct the reduced basis via the POD and the GP surrogate, $N=40$ samples are arranged
 166 in a Latin hypercube over $m \in [0, 12]$ and $\alpha \in [0, 3]$ (see the left plot in Figure 2). We then run
 167 the FE solver (implemented in **Firedrake** (Rathgeber et al., 2016)) of the toy problem to obtain
 168 the corresponding 2-D outputs, each of which contains FE solutions on $K = 78961$ nodes. These
 169 40×78961 high-dimensional outputs are then reduced to 40 low-dimensional outputs (40×25)
 170 using POD by retaining the first 25 principal components out of the total 40 components, see
 171 the right plot in Figure 2, where the cumulative explained variance is defined as $\frac{\sum_{i=1}^L \lambda_i}{\sum_{i=1}^N \lambda_i}$ with L
 172 be the number of components.

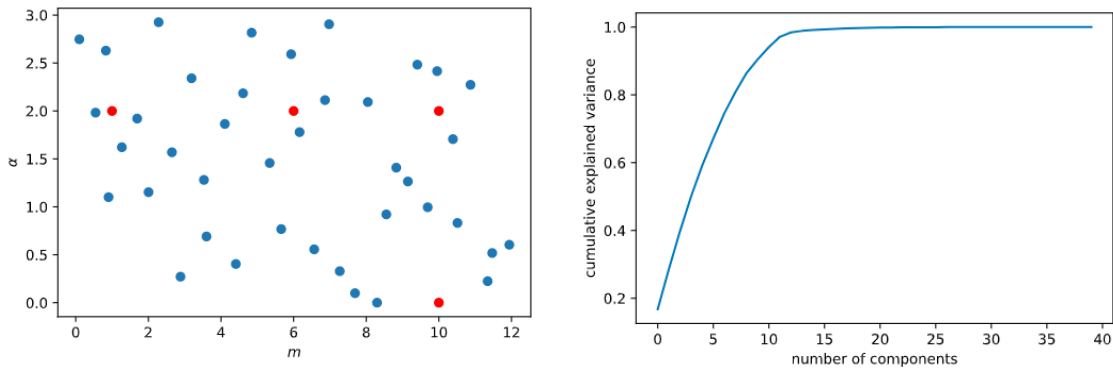


Figure 2: (*Left*): Training and designing points generated for the inputs m and α . The blue points are design input locations generated from the Latin hypercube design and the red points are testing input locations; (*Right*): cumulative explained variance given by the POD.

173 GP surrogates are then constructed independently for each of the 25 dimensions of the
 174 reduced order data. GP surrogates are trained with the Matérn-2.5 kernel using the **RobustGASP**
 175 package in R.

176 3.1.2 Experimental Results

177 We test the constructed non-intrusive ROM at four testing input positions $(m, \alpha) = (6, 2)$,
 178 $(10, 2)$, $(1, 2)$ and $(10, 0)$ (see the left plot of Figure 2). The FE solutions (from the **Firedrake**)
 179 and the predicted solutions from the built ROM are compared in Figure 3. The normalised (to
 180 the range of FE solutions) errors between the FE solutions and the predicted solutions from the
 181 built ROM are shown in Figure 4. The coverage of the ROM (i.e., the instances that the FE
 182 solutions fall within the predictive bounds of GP-based ROM) are also given in Figure 5.

183 It can be seen from these results that the constructed ROM with GP could predict well
 184 the FE solutions of the anisotropic problem at input locations that are not realised. Among
 185 the four testing positions, the final case with $m = 10$ and $\alpha = 0$ presents the largest normalised
 186 errors up to 13%. This is not a surprising result because m has no effect on the FE solution of
 187 the problem when $\alpha = 0$. However, this information is not fully captured in the training data
 188 and thus not gained by the non-intrusive ROM with GP, which is pure data-driven method that
 189 only understands the functional relation between m , α and the solution field from the training
 190 set. As a result, we could observe 5 blurred oscillation periods in the predicted solutions from

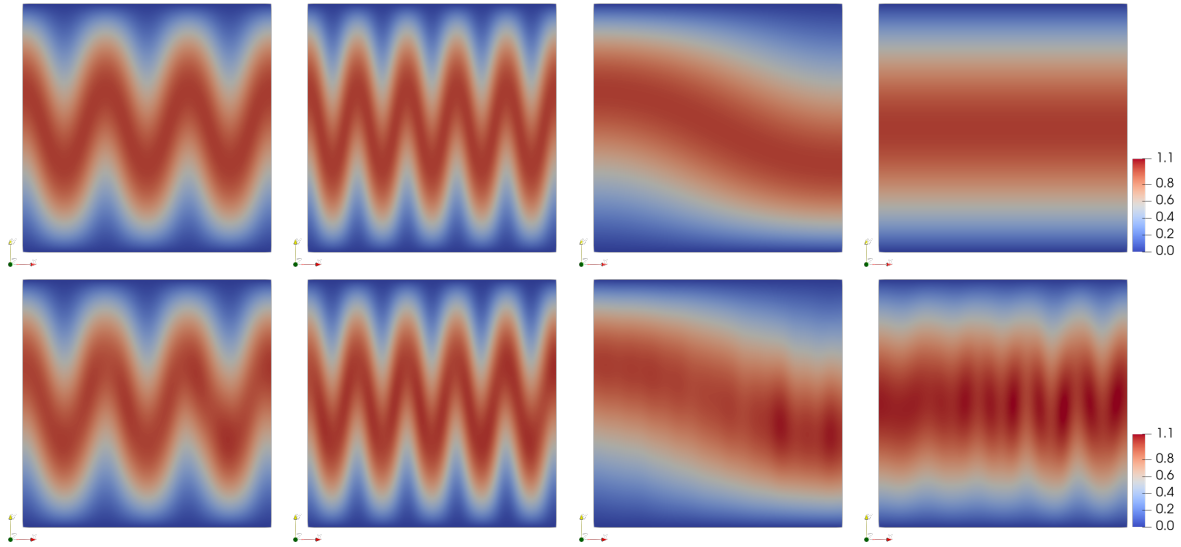


Figure 3: Comparisons of FE solutions to the predicted solutions given by the constructed GP-based ROM. The first row gives the FE solutions. The second row gives the predicted solutions from the GP-based ROM. The columns from left to right correspond to testing input positions $(m, \alpha) = (6, 2), (10, 2), (1, 2)$ and $(10, 0)$ respectively.

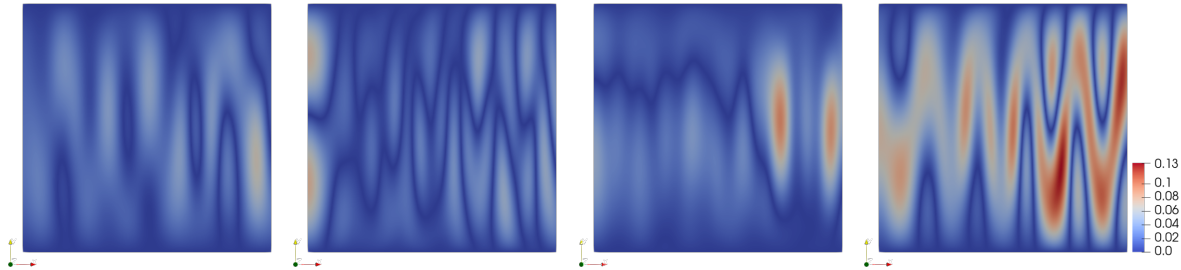


Figure 4: The normalised errors between FE solutions and the predicted solutions from the ROM with GP surrogate. The plots from left to right correspond to testing input positions $(m, \alpha) = (6, 2), (10, 2), (1, 2)$ and $(10, 0)$ respectively.

191 ROM in Figure 3. However, the predictive interval (whose upper and lower bounds are given
 192 at two standard deviations $2\hat{\sigma}$ above and below the predictive mean $\hat{\mu}$) of the GP-based ROM
 193 covers the FE solutions sufficiently in this case, demonstrating that one can benefit from the
 194 predictive uncertainty embedded in the non-intrusive ROM coupled with GP emulation.

195 4 Active learning for Non-intrusive ROM with Gaussian Pro- 196 cess Surrogates

197 4.1 Why Active Learning?

198 Active learning, also known as sequential design, is a collection of approaches that adaptively
 199 enrich the training points for surrogate modelling of computer solvers. In comparison to one-

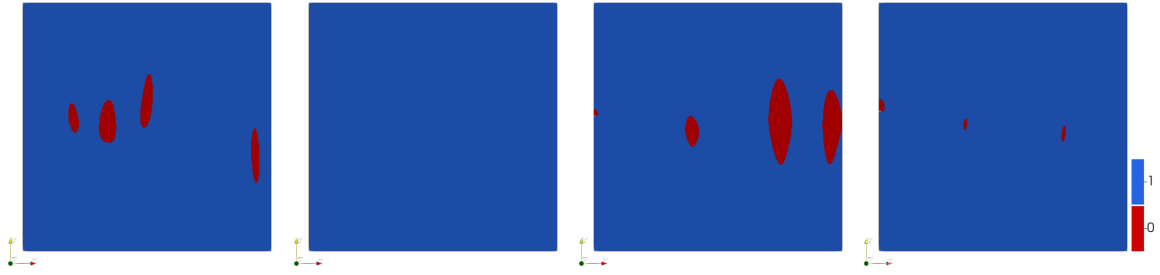


Figure 5: The coverage of constructed ROM with GP, giving the instances that FE solutions fall within the predictive bounds provided by the ROM with GP. 1 indicates that the FE solution is covered by the predictive interval (whose upper and lower bounds are given at two standard deviations $2\hat{\sigma}$ above and below the predictive mean $\hat{\mu}$) and 0 indicates otherwise. The plots from left to right correspond to testing input positions $(m, \alpha) = (6, 2), (10, 2), (1, 2)$ and $(10, 0)$ respectively.

200 shot designs, such as Latin-hypercube designs (LHD), the active learning is preferred in many
 201 cases:

- 202 • One wants a proper utilisation of computational resources. Active learning allows one to
 203 choose computer model input locations adaptively, and therefore can monitor the quality
 204 of the resulting surrogate model while the active learning is in progress and determine
 205 whether to pause or continue the model evaluations;
- 206 • More computer model evaluations are needed in the input region of interest. Unlike static
 207 space-filling designs, such as LHD, active learning, depending on the quality of the under-
 208 lying surrogate model (as we will discuss in Section 4.4), could direct the computer models
 209 to evaluate at input locations where the model response exhibits more variations and thus
 210 are more of interest;
- 211 • There are existing computer model evaluations, but are potentially large in size and/or
 212 not produced with a careful design. It can be computationally inefficient to generate a
 213 new design, e.g., a static space-filling design, if one has an existing set of model evaluations
 214 because one could utilise the data available. However, it can be both numerically inefficient
 215 (e.g., the design formed by the existing data is poor) and computationally burdensome
 216 (e.g., the existing data is of large size) to use the whole existing model realisations for
 217 surrogate modelling. Thus, one can use active learning to choose training data adaptively
 218 from the existing model evaluations from a small design size while at the same time prevent
 219 from the numerical instabilities induced by poor designs;
- 220 • There is a system of coupled computer models. It has been shown in Ming and Guillas
 221 (2021) that active learning is essential to construct Gaussian process (GP) based surrogate
 222 models in a computationally efficient and effective manner. Static designs of global inputs
 223 can produce poor designs, and thus numerical issues, to sub-models of a computer system,

224 and can also waste computational resources over input regions of sub-models that are not
 225 contributing to the global outputs (that correspond to the global input region of interest).

226 4.2 Implementation

227 Assume that we have data $\mathcal{D}_n = \{\mathbf{X}_n, \mathbf{Y}_n\}$ that consists of input $\mathbf{X}_n \in \mathbb{R}^{n \times D}$ and the responding
 228 high-dimensional computer model output $\mathbf{Y}_n \in \mathbb{R}^{n \times K}$. Then, a generic active learning procedure
 229 that selects the next input position \mathbf{x}_{n+1} to be evaluated by the computer model for refinement
 230 of GP based non-intrusive ROM (abbreviated as GP-ROM in the remainder of the report)
 231 introduced in Section 3 is given in Algorithm 1. Once \mathbf{x}_{n+1} is determined, one can then obtain
 232 the augmented data $\mathcal{D}_{n+1} = \{\mathbf{X}_{n+1}, \mathbf{Y}_{n+1}\}$ by concatenating \mathbf{x}_{n+1} and its corresponding high-
 233 dimensional output \mathbf{y}_{n+1} to \mathcal{D}_n and update GP-ROM $\{\mathcal{GP}_l\}$ by re-invoking Algorithm 1.

Algorithm 1 Active learning for GP-ROM

Input: (i) $\mathcal{D}_n = \{\mathbf{X}_n, \mathbf{Y}_n\}$; (ii) a candidate set \mathcal{C} of input locations $\{\mathbf{x}_i\}_{i=1,\dots,M}$.

Output: The next input position \mathbf{x}_{n+1} to be evaluated by the computer model.

- 1: Compute the low-dimensional output $\hat{\mathbf{Y}}_n \in \mathbb{R}^{n \times L}$ of \mathbf{Y}_n and the corresponding eigenvalues $\lambda_{l=1,\dots,L}$ using POD;
- 2: Construct GP-ROM $\{\mathcal{GP}_l\}$ using $\{\mathbf{X}_n, \hat{\mathbf{Y}}_n\}$;
- 3: Calculate the criterion $I_l(\mathbf{x})$ at each input locations in \mathcal{C} using \mathcal{GP}_l for all l ;
- 4: Choose for the next input position \mathbf{x}_{n+1} by solving

$$\mathbf{x}_{n+1} = \operatorname{argmax}_{\mathbf{x} \in \mathcal{C}} \sum_{l=1}^L w_l I_l(\mathbf{x}) \quad \text{with} \quad w_l = \frac{\lambda_l}{\sum_{i=1}^L \lambda_i}$$

We present two candidates for the criterion $I_l(\mathbf{x})$ based on the Active Learning MacKay (ALM) (MacKay, 1992) and the Active Learning Cohn (ALC) (Cohn, 1996) respectively for the selection of \mathbf{x}_{n+1} . ALM aims to find the next input location that corresponds to the maximum predictive variance exhibited by the GP-ROM. Thus, $I_l(\mathbf{x})$ is defined by

$$I_l(\mathbf{x}) = \hat{\sigma}_l^2(\mathbf{x}),$$

where $\hat{\sigma}_l^2(\mathbf{x})$ is the posterior predictive variance of \mathcal{GP}_l evaluated at \mathbf{x} . However, ALM has a well-know issue that it selects excessive input locations around boundaries of the input region because of the lack of data beyond boundaries. To alleviate this issue, ALC aims to select the input position such that the integrated predictive variance of GP-ROM over the input region is minimised after augmenting \mathbf{x}_{n+1} to \mathbf{X}_n . Formally, $I_l(\mathbf{x})$ under ALC is defined by

$$I_l(\mathbf{x}) = - \int_{\mathbf{x}^* \in \mathcal{X}} \hat{\sigma}_l^2(\mathbf{x}^* | [\mathbf{X}_n^\top, \mathbf{x}^\top]^\top) d\mathbf{x}^*.$$

234 where $\hat{\sigma}_l^2(\mathbf{x}^* | [\mathbf{X}_n^\top, \mathbf{x}^\top]^\top)$ is interpreted as the posterior predictive variance of \mathcal{GP}_l evaluated at
 235 \mathbf{x}^* given the input data \mathbf{X}_n being augmented by \mathbf{x}_n . It is worth noting that the computation of
 236 $\hat{\sigma}_l^2(\mathbf{x}^* | [\mathbf{X}_n^\top, \mathbf{x}^\top]^\top)$ does not require evaluations of the associated computer model at \mathbf{x}_n because
 237 the predictive variance of GP does not depend on the output data. In practice, the integral
 238 involved in ALC can be approximated by the Monte Carlo integration over a reference set \mathcal{X}

239 (that can be the same as the candidate set \mathcal{C}) generated by the LHD. To implement a full active
 240 learning procedure, one often starts with a small data set that is generated by a static design,
 241 such as LHD, and then execute T iterations of Algorithm 1 to enrich the initial data set with T
 242 additional realisations from the computer model.

243 4.3 Active learning for the GP-ROM emulation of the 2-D anisotropic heat 244 transport model

245 In this section, we demonstrate how efficiency gains can be made using active learning for the
 246 GP-ROM of the FE solver to the 2-D problem described in Section 3.1

247 4.3.1 Experimental Setup

To initiate the active learning to build GP-ROM, $N=20$ initial training data points, whose input locations are generated via the LHD over $m \in [0, 12]$ and $\alpha \in [0, 3]$ with the corresponding 2-D output (that contains $K = 78961$ solution nodes) determined by running the FE solver (implemented in `Firedrake` (Rathgeber et al., 2016)). We then iterate Algorithm 1 for both ALM and ALC 80 times to augment additional 80 training data points to the initial data set. At each iteration of the active learning, we choose the number of components L (in Line 1 of Algorithm 1) to be retained from POD based on the following criteria:

$$L = \operatorname{argmin}_{L^* \in \{1, \dots, n\}} \left| \frac{\sum_{i=1}^{L^*} \lambda_i}{\sum_{i=1}^n \lambda_i} - 0.9998 \right|,$$

where $\lambda_1 > \lambda_2 > \dots > \lambda_n$. To take into account the effects of initial data set on the active learning, we repeat both ALM- and ALC-based active learning 10 times. For the comparison between ALM and ALC, we generate 2500 testing data points over $m \in [0, 12]$ and $\alpha \in [0, 3]$ and compute the Normalised Root Mean Squared Error (NRMSE) at each active learning iteration by

$$\text{NRMSE} = \frac{1}{2500} \sum_{i=1}^{2500} \frac{\sqrt{\frac{1}{K} (\tilde{\mathbf{z}}_i - \mathbf{z}_i)(\tilde{\mathbf{z}}_i - \mathbf{z}_i)^\top}}{\max(\mathbf{z}_i) - \min(\mathbf{z}_i)} \times 100\%,$$

248 where $\tilde{\mathbf{z}}_i \in \mathbb{R}^{1 \times K}$ and $\mathbf{z}_i \in \mathbb{R}^{1 \times K}$ are 2-D FE solution fields generated by the GP-ROM and
 249 `Firedrake` at the i -th testing input location, respectively.

250 In terms of implementation, we construct GP-ROM and compute corresponding ALM and
 251 ALC criteria at each iteration of the active learning using the `laGP` package in R.

252 4.3.2 Experimental Results

253 Figure 6 presents the NRMSEs of GP-ROMs built with ALM- and ALC-based active learning
 254 over 80 iterations, in comparison to those constructed with the static LHD at various design
 255 sizes. It can be observed that for design size less than 50, GP-ROMs trained using the active
 256 learning, regardless of ALM or ALC, provide higher accuracy than those trained using the static
 257 LHD. However, as the design sizes increases, the accuracy of GP-ROMs built by the active
 258 learning and LHD are comparable. This is because with a large design size, the input domain is

259 densely space-filled by the LHD and thus the NRMSE of the corresponding GP-ROM converges
 260 to that of the GP-ROM trained with the active learning.

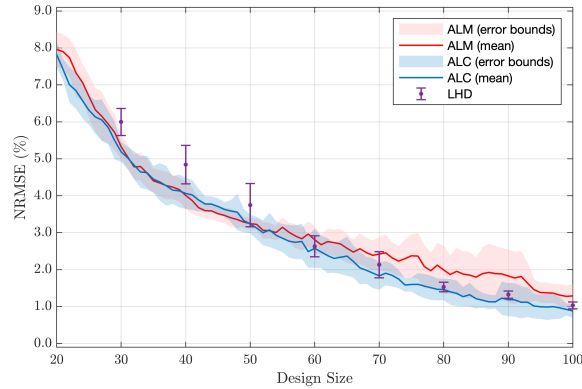


Figure 6: Comparison of NRMSEs of GP-ROM constructed using the ALM-based active learning, the ALC-based active learning, and the static LHD.

261 We also observe from Figure 6 that for design size larger than 60 GP-ROMs constructed by
 262 LHD perform better (in terms of overall lower NRMSE) than those built by ALM-based active
 263 learning. This observation can be explained by the fact that ALM-based active learning has
 264 the tendency to choose excessive input locations around boundaries of the input domain (see
 265 Figure 7(a)) and thus could fail to achieve a satisfactory design, in which input locations are
 266 preferred to be scattered within the input domain of interest (see Figure 7(b)).

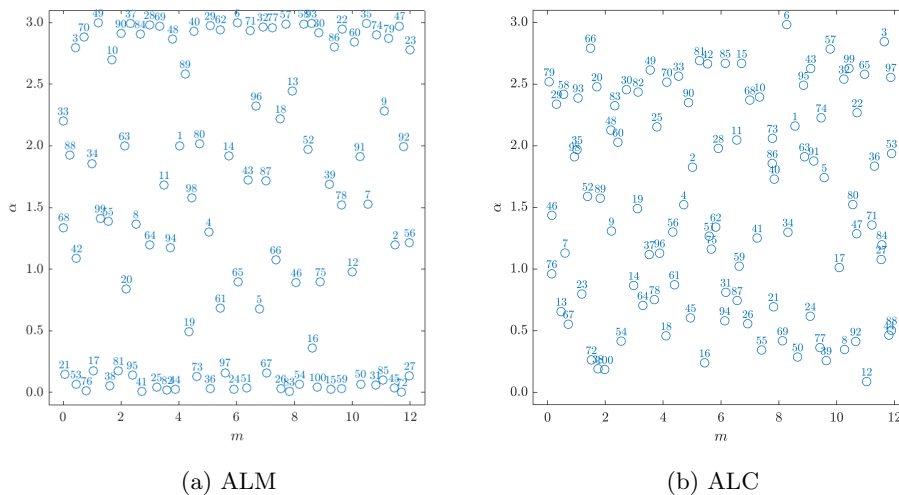


Figure 7: Designs produced by a random trial (out of 10 repeated trials) of ALM- and ALC-based active learning.

267 4.4 Discussion

268 In this section, we introduce a simple and effective procedure to implement the active learning
 269 for GP-ROM construction. Although the active learning may eventually produce a space-filling
 270 design, it gives the computer model experimenters more controls over their computational re-

271 sources. One may criticise that active learning is not computationally efficient in the sense that
272 it directs model runs sequentially and thus can be time-consuming in comparison to static one-
273 shot designs in which model runs can be done in parallel. This statement is sensible when one
274 posses sufficient computational power (for parallel computing) and active learning also produces
275 a space-filling design. However, in real-world data these conditions may not be fulfilled. Our
276 computational resources may not permit us to obtain model realisations that cover adequately
277 the input region of interest (for an accurate surrogate model) and a space-filling design may
278 not capture sufficiently (without tremendous computational efforts) the input regions where the
279 model response exhibits abrupt changes, even if we have an advanced surrogate model (that is
280 suitable for both stationary and non-stationary data). On the contrary, active learning has the
281 ability to focus on input regions where the corresponding output surfaces show more variations,
282 given that the underlying surrogate model provides a satisfactory uncertainty quantification (e.g.,
283 highlighting the regions with higher predictive standard deviations). A fact often forgotten in
284 computer model experiments is that design and surrogate modelling are not two separate tasks.
285 Good designs produce good surrogates with less numerical issues and more reliable uncertainty
286 quantification, which in turn induces designs that better represent the functional behaviours of
287 computer models under the consideration. These are the reasons why active learning could be
288 preferred to static space-filling designs, which could cause the surrogate modelling challenging
289 (e.g., a large number of realisations that are needed to capture well the computer model can
290 cause the GP-ROM computationally prohibitive) and do not utilise the uncertainties quantified
291 by surrogate models for design improvement.

292 It is worth noting that active learning does not guarantee the locations of (possibly very
293 small but important) input regions of a computer model that correspond to abrupt changes
294 to the model responses. The design produced by the active learning depends on the quality
295 of the underlying surrogate model, which in turn depends on the information contained in
296 the training data (assuming that the surrogate represents the training data adequately and
297 produces sensible uncertainty quantification). Therefore, whether active learning could find
298 input regions that has very localised and important features depends on if the information of
299 the regions exists in the training data. For this reason, it is vital to have a good initial design
300 that incorporates such information for the active learning. However, in practice this can be
301 difficult to achieve, particularly for high-dimensional cases, even we have some prior knowledge
302 that such non-stationary features exist in the computer model, and as a consequence we may
303 obtain a surrogate that completely ignores these regions with significant computational costs
304 being wasted. To alleviate this issue, one could simply evaluate the computer model with a high-
305 resolution design using the parallel computing. In this way, the local behaviours of a computer
306 model can be captured within a reasonable amount of time. Nevertheless, it is not advisable to
307 use all model evaluations for surrogate modelling, especially for GP-based surrogates because the
308 large amount of data can cause GP surrogates computationally prohibitive and some evaluations
309 (e.g., that form a flat response surface) are redundant for surrogate improvement. As a result,
310 we propose the following hybrid static-active learning procedure to address the scenario in which
311 we aim to construct efficiently (in terms of computation and time) a surrogate model that could
312 mimic the underlying computer model with localised behaviours:

- 313 1. Generate a data set by evaluating the computer model over a dense space-filling design in
314 parallel;
- 315 2. Choose a subset of the produced data set as the initial design for the active learning;
- 316 3. Implement the active learning that adaptively refines the design and the surrogate model,
317 e.g., GP-ROM, by selecting data points from the data set produced in Step 1.

318 There are several benefits provided by the above procedure. Firstly, the high-resolution design
319 provides some guarantees that our data contain information of localised behaviours embedded in
320 the underlying computer model. In addition, unlike typical active learning that evaluates models
321 sequentially, active learning in Step 3 uses the data set already generated with a parallelisable
322 strategy and thus could save a considerable amount of time (especially when computer models
323 are very expensive to run). Furthermore, with active learning one is able to pick (potentially
324 a small amount of) data points (from the generated data set) that contribute most to the
325 surrogate quality, instead of naively pouring the whole data set into the surrogate construction
326 (causing computational difficulties). Perhaps the most decisive and challenging step of the
327 above procedure is Step 2 because, as discussed, one expects to incorporate some information of
328 localised behaviours of a computer model into the initial design such that the resulting surrogate
329 is less likely to overlook these features. How to integrate experts' knowledge about the localised
330 features into the initial design is worth exploring in the future, but the procedure above indicates
331 a potentially brutal but simply implementation for Step 2: choose multiple random subsets of the
332 data set, then proceed to Step 3 for multiple surrogate constructions, and choose the surrogate
333 that gives the best predictive accuracy (e.g., lowest overall predictive error against the generated
334 data set). This implementation is computationally efficient because active learnings in Step 3
335 initiated by different random designs can be executed in parallel and do not involve computer
336 model evaluations.

337 5 Future Directions

338 We demonstrate in this report that a GP-ROM could be used to replace computationally expen-
339 sive computer solvers for problems with high-dimensional output, in one of the building blocks of
340 nuclear fusion modelling. However, dimension reduction techniques such as POD lose informa-
341 tion when the original data are projected onto a lower dimensional space, and thus some extreme
342 but important events could be masked in the low dimensional data, a scenario called masking
343 effect. As a result, if the surrogate is built on the low dimensional data one may not be able to
344 recover these outlying events using the constructed non-intrusive ROM. Therefore, other dimen-
345 sion reduction methods that may be more resistant to the masking effect could be examined.
346 In addition, although GP-ROM requires no domain knowledge and access to the source code of
347 original problems, it ignores the physics implied by the underlying problem and thus may be
348 inaccurate comparing to the its intrusive counter-party. Therefore, it would be worth exploring
349 the trade-off between the speed and accuracy of intrusive and non-intrusive MOR, especially
350 in context of UQ. It would also be interesting to find a middle ground where one could exploit
351 the benefits (e.g., accuracy, speed and uncertainty) of both intrusive and non-intrusive ROM,

352 producing a physics-informed non-intrusive ROM. Some relevant literature on physics-informed
353 machine learning (say using a boundary condition or other approaches) include Vernon et al.
354 (2019); Kashinath et al. (2021); Watson-Parris (2021).

355 **Recommendation:** Investigate how to apply physics-informed GP-ROM in key nuclear fusion
356 models. Examine how to build new types of GP-ROM for the case of particle-based models (PIC)
357 whose outputs need to be understood as a continuum.

358 5.1 Deep GP for Non-intrusive ROM

359 In this report we explored how to construct GP-ROM using active learning. Active learning
360 is particularly useful when the underlying computer model exhibits non-stationary features
361 as it has the ability to produce a non-uniform design that appreciates the non-stationarity.
362 However, the success of the active learning relies on the quality of uncertainty quantified by
363 the surrogate model. Since conventional GP surrogates assume stationarity, more advanced
364 non-stationary GP models, such as deep Gaussian processes (Damianou and Lawrence, 2013),
365 would be good candidates for non-intrusive ROM of fusion models that exhibits non-stationarity.
366 Deep Gaussian processes (DGPs) are feed-forward compositions of conventional stationary GPs
367 with flexible model expressiveness, particularly for non-stationary data. However, training and
368 prediction of DGP based emulators are challenging due to the non-linearity induced by the kernel
369 functions involved in GPs. Various inference methods thus are introduced to tackle this issue.
370 Variational inferences, such as Doubly Stochastic Variational Inference (DSVI) (Salimbeni and
371 Deisenroth, 2017), is computationally thrifty but is not accurate because simplified assumptions
372 over the latent variables in DGP hierarchy are assumed. On the contrary, the fully-Bayesian
373 approach introduced by Sauer et al. (2020) gives a comprehensive uncertainty quantification
374 of DGPs, but at the expense of computation. The stochastic imputation approach recently
375 proposed by Ming et al. (2021) is a DGP inference method that enjoys both computational
376 speed and the predictive accuracy, and could be a competitive and potential candidate for DGP
377 emulations of non-stationary fusion models. It is implemented in the `dgpsi` package¹.

378 Figure 8 showcases the ALM-based active learning using a two-layered DGP surrogate (i.e.,
379 composition of two stationary GPs) trained with the stochastic imputation in comparison to that
380 using a stationary GP. It can be observed that DGP surrogate outperforms the GP surrogate in
381 both mean predictions and uncertainty quantification. In addition, with DGP the active learning
382 could produce a non-uniform design that appreciates the non-stationarity of the underlying data.
383 While the active learning essentially produces a quite space-filling design under GP, it assigns
384 three time more number of design points to the rough (and more interesting) regime over $[0, 0.5]$
385 than the flat regime over $(0.5, 1]$ under DGP. Although this is a simple 1-D example, it gives
386 motivations why DGP surrogate should be seriously considered if the reduced-order output of a
387 fusion model is non-stationary and the active learning is employed.

388 **Recommendation:** Investigate how to reduce dimensionality of outputs for key nuclear fusion
389 models whose behaviour may present sharp transitions or various regimes, such as turbulence
390 models. The key question is then how to understand and represent the continuum of outputs

¹<https://github.com/mingdeyu/DGP>

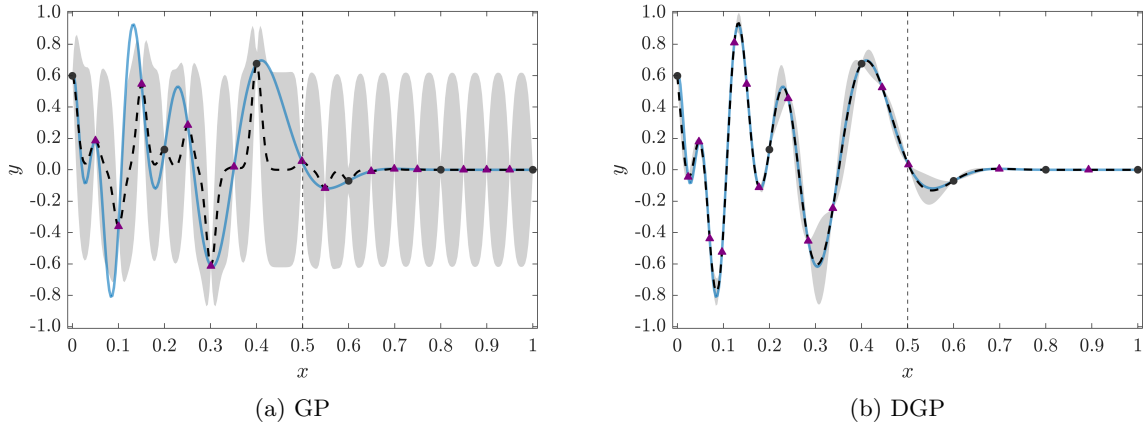


Figure 8: ALM-based active learning using GP and DGP emulations. Solid line represents the underlying true function; Dashed line is the mean prediction; Shaded area represents 95% predictive interval; Dots (6 in total) are initial training points and triangles (14 in total) are training points enriched by the active learning procedure using GP and DGP surrogates. The vertical dashed line indicates a visual split of the underlying true function into a rough regime over $[0, 0.5]$ and a flat regime over $(0.5, 1]$.

391 features across regimes. Indeed these features shown in 3 can vary across regimes and must
 392 be made consistent by some form of joint augmentation possibly at a small cost but with large
 393 benefits for emulation.

394 5.2 Active subspace for efficient dimension reduction of inputs

395 The efficiency of reducing dimensions in the inputs was demonstrated in Liu and Guillas (2017).
 396 Gains of orders of magnitude can be achieved. For instance, the application to a surface of
 397 inputs (a mesh of 3200 elements) enabled a reduction from dimension 3200 to 5 with fast and
 398 accurate emulation. Only about 100 simulations were needed to come up with 5 key dimensions
 399 as a recombination of the original 3200 dimensions. A summary of the method is presented
 400 below. It is implemented in the Alan Turing Institute Package *Multi-Output Gaussian Process*
 401 *Emulator* (MOGP)². The context is:

- 402 • Simulator input X (high dimension \mathbb{R}^p) and output $Y = f(X)$ (one dimension \mathbb{R}^1)
- 403 • GP emulation: fit an GP and predict $f(x_{new})$ using a sample of simulations $f(X_1), \dots, f(X_n)$
- 404 • Find a reduced space (known as sufficient dimension reduction SDR) $R(X) \in \mathbb{R}^d$, $d < p$,
 405 such that there is (nearly) no loss of information in predicting Y by providing $R(X)$ instead
 406 of X
- To achieve SDR, employ the gradient-based Kernel Dimension Reduction (gKDR) ap-
 proach (Fukumizu and Leng, 2014):

$$R(X) = B^T X, \quad B^T B = I_d, \quad d < p.$$

²<https://github.com/alan-turing-institute/mogp-emulator>

407 Estimate B from simulation samples $(X_1, Y_1), \dots, (X_n, Y_n)$. Note that no strong assumption
 408 are made on the variables (type, distribution, dimension).

409 The specific technical steps in gKDR involve two Reproducing kernel Hilbert spaces (RKHS):

- 410 • Prepare kernels $k_{\mathcal{X}}$ and $k_{\mathcal{Y}}$, with the associated (RKHS) $\mathcal{H}_{\mathcal{X}}$ and $\mathcal{H}_{\mathcal{Y}}$
- 411 • The quantities of interest are the gradients $\frac{\partial E[g(Y)|X]}{\partial X}$ for any $g \in \mathcal{H}_{\mathcal{Y}}$ as their evaluation
 412 is the ingredient for the identification of the reduced subspace, by looking at the most
 413 influential directions.
- Estimate (see Fukumizu and Leng (2014) for details)

$$\hat{M}_n = \frac{1}{n} \sum_{i=1}^n \nabla \mathbf{k}_{\mathcal{X}}(X_i)^T (G_X + n\epsilon_n I)^{-1} G_Y (G_X + n\epsilon_n I)^{-1} \nabla \mathbf{k}_{\mathcal{X}}(X_i)$$

414 where G_X and G_Y are the Gram matrices $(k_{\mathcal{X}}(X_i, X_j))$ and $(k_{\mathcal{Y}}(Y_i, Y_j))$, and $\nabla \mathbf{k}_{\mathcal{X}}(x) =$
 415 $(\partial k_{\mathcal{X}}(X_1, x)/\partial x, \dots, \partial k_{\mathcal{X}}(X_n, x)/\partial x)^T \in \mathbb{R}^{n \times m}$ for any $x \in \mathbb{R}^m$.

- Eigen-decompose \hat{M}_n into $\hat{M}_n = \hat{Q} \hat{\Lambda} \hat{Q}^T$ and partition

$$\hat{\Lambda} = \begin{bmatrix} \hat{\Lambda}_1 & \\ & \hat{\Lambda}_2 \end{bmatrix}, \quad \hat{Q} = [\hat{B} \quad \hat{C}],$$

416 where $\hat{\Lambda}_1 = \text{diag}(\hat{\lambda}_1, \dots, \hat{\lambda}_d)$ consisting of the first d largest eigenvalues, to ultimately
 417 provide the dimension reduction.

418 The emulation with dimension reduction can be carried out and its loss quantified (Liu and
 419 Guillas, 2017):

- 420 • $f(X) \approx \hat{f}(\hat{B}^T X)$

$$\begin{aligned} 421 & \quad \left\| f - \hat{f} \right\|_{L_2} = \\ 422 & \quad O_p \left(\frac{4}{\lambda_d - \lambda_{d+1}} n^{-\min\{\frac{1}{3}, \frac{2\beta+1}{4\beta+4}\}} \left(\sum_{i=1}^d c_i \hat{\lambda}_i^2 \right)^{\frac{1}{2}} + \left(\sum_{i=d+1}^m c_i \hat{\lambda}_i^2 \right)^{\frac{1}{2}} \right) \end{aligned}$$

- 423 • Build emulator $\tilde{f} \approx \hat{f}$ on low dimensional space $\hat{B}^T X$
- Approximation procedure:

$$f(X) \approx \hat{f}(\hat{B}^T X) \approx \tilde{f}(\hat{B}^T X)$$

424 The choice of remained dimension d and hyperparameters is performance based (e.g. in the
 425 quality of the predictions in a leave-one-out strategy) and can result in very large gains (Liu
 426 and Guillas, 2017).

427 **Recommendation:** Investigate how to reduce dimensionality of inputs of key nuclear fusion
 428 models such as the magnetic field modelled input of the anisotropic heat transfer model.

447 construct the non-intrusive ROM of the whole system by linking the non-intrusive ROM of f_1
448 to that of f_2 through the reduced space w analytically. One key benefit of this approach for
449 system-wise reduced order modelling is that one only needs to do dimensionality reduction to
450 the outputs of sub-models. Whereas, to build intrusive ROM, one has to make extra challenging
451 efforts to reformulate the original high-fidelity model f_2 under reduced input w and output y .

452 Implementing the active learning for linked GP surrogates for systems of computer models
453 with high-dimensional outputs is also challenging. In comparison to the static design (in which
454 the training input data of one sub-model matches the training output data produced by the
455 feeding sub-models), the active learning (e.g., the adaptive design introduced in Ming and Guillas
456 (2021)) could lose the input/output data matching, and thus further explorations are required
457 to examine how to conduct dimension reductions for the internal sub-model input/output so
458 that all information contained in the training data of linked sub-models are utilised.

459 **Recommendation:** Investigate how to jointly reduce dimensionality of outputs that are inputs
460 of key nuclear fusion models, such as the heat from the anisotropic heat transfer model propa-
461 gated to the wall heat transfer model. Emulation with high-dimensional outputs (GP-ROM) of
462 the first simulator and active subspace for dimension reduction of the subsequent inputs of the
463 following simulator should be used in synergy. To establish such a combined strategy will require
464 examining carefully how to weigh variations in outputs of the first model and the influence of
465 inputs for the second. The sampling approach of 4 needs to be tailored to this new context as
466 well. It is necessary to carry out such combination of methods and strategies due to the very
467 high dimensions, heavy data transfers, and extremely costly simulations.

468 References

- 469 Chang, K.-L., Guillas, S., et al. (2019). Computer model calibration with large non-stationary
470 spatial outputs: application to the calibration of a climate model. *Journal of the Royal*
471 *Statistical Society Series C*, 68(1):51–78.
- 472 Cohn, D. A. (1996). Neural network exploration using optimal experiment design. *Neural*
473 *networks*, 9(6):1071–1083.
- 474 Dalbey, K. R. (2013). Efficient and Robust Gradient Enhanced Kriging Emulators. Technical
475 Report SAND2013–7022, Sandia National Laboratories: Albuquerque, NM, USA.
- 476 Damianou, A. and Lawrence, N. D. (2013). Deep Gaussian processes. In *Artificial intelligence*
477 *and statistics*, pages 207–215. PMLR.
- 478 Deluzet, F. and Narski, J. (2019). A two field iterated asymptotic-preserving method for highly
479 anisotropic elliptic equations. *Multiscale Modeling & Simulation*, 17(1):434–459.
- 480 Fukumizu, K. and Leng, C. (2014). Gradient-based kernel dimension reduction for regression.
481 *Journal of the American Statistical Association*, 109(505):359–370.
- 482 Gu, M. and Berger, J. O. (2016). Parallel partial Gaussian process emulation for computer
483 models with massive output. *The Annals of Applied Statistics*, 10(3):1317–1347.

- 484 Gu, M., Palomo, J., and Berger, J. O. (2018a). RobustGaSP: robust Gaussian stochastic process
485 emulation in R. *arXiv:1801.01874*.
- 486 Gu, M., Wang, X., and Berger, J. O. (2018b). Robust Gaussian stochastic process emulation.
487 *The Annals of Statistics*, 46(6A):3038–3066.
- 488 Guillas, S., Sarri, A., Day, S. J., Liu, X., Dias, F., et al. (2018). Functional emulation of high
489 resolution tsunami modelling over Cascadia. *Annals of Applied Statistics*, 12(4):2023–2053.
- 490 Kashinath, K., Mustafa, M., Albert, A., Wu, J., Jiang, C., Esmailzadeh, S., Azizzadenesheli,
491 K., Wang, R., Chattopadhyay, A., Singh, A., et al. (2021). Physics-informed machine learning:
492 case studies for weather and climate modelling. *Philosophical Transactions of the Royal Society
493 A*, 379(2194):20200093.
- 494 Kyzyurova, K. N. (2017). *On uncertainty quantification for systems of computer models*. PhD
495 thesis, Duke University.
- 496 Liu, H., Ong, Y.-S., Shen, X., and Cai, J. (2020). When Gaussian process meets big data:
497 a review of scalable GPs. *IEEE transactions on neural networks and learning systems*,
498 31(11):4405–4423.
- 499 Liu, X. and Guillas, S. (2017). Dimension reduction for Gaussian process emulation: An appli-
500 cation to the influence of bathymetry on tsunami heights. *SIAM/ASA Journal on Uncertainty
501 Quantification*, 5(1):787–812.
- 502 MacKay, D. J. (1992). Information-based objective functions for active data selection. *Neural
503 computation*, 4(4):590–604.
- 504 Ming, D. and Guillas, S. (2021). Linked Gaussian process emulation for systems of computer
505 models using Matérn kernels and adaptive design. *SIAM/ASA Journal on Uncertainty Quan-
506 tification (in press)*. *ArXiv preprint arXiv:1912.09468*.
- 507 Ming, D., Williamson, D., and Guillas, S. (2021). Deep gaussian process emulation using stochas-
508 tic imputation. *arXiv:2107.01590*.
- 509 Pedregosa, F., Varoquaux, G., Gramfort, A., Michel, V., Thirion, B., Grisel, O., Blondel, M.,
510 Prettenhofer, P., Weiss, R., Dubourg, V., Vanderplas, J., Passos, A., Cournapeau, D., Brucher,
511 M., Perrot, M., and Duchesnay, E. (2011). Scikit-learn: Machine learning in Python. *Journal
512 of Machine Learning Research*, 12:2825–2830.
- 513 Quarteroni, A., Manzoni, A., and Negri, F. (2015). *Reduced Basis Methods for Partial Differ-
514 ential Equations: An Introduction*, volume 92. Springer.
- 515 Rasmussen, C. E. and Williams, C. K. (2006). *Gaussian Processes for Machine Learning*. The
516 MIT Press, Cambridge, MA.
- 517 Rathgeber, F., Ham, D. A., Mitchell, L., Lange, M., Luporini, F., McRae, A. T., Bercea, G.-T.,
518 Markall, G. R., and Kelly, P. H. (2016). Firedrake: automating the finite element method by
519 composing abstractions. *ACM Transactions on Mathematical Software (TOMS)*, 43(3):1–27.

- 520 Roustant, O., Ginsbourger, D., and Deville, Y. (2012). DiceKriging, DiceOptim: two R packages
521 for the analysis of computer experiments by kriging-based metamodeling and optimization.
522 *Journal of Statistical Software*, 51(i01).
- 523 Salimbeni, H. and Deisenroth, M. (2017). Doubly stochastic variational inference for deep
524 Gaussian processes. In *Advances in Neural Information Processing Systems*, pages 4588–4599.
- 525 Sauer, A., Gramacy, R. B., and Higdon, D. (2020). Active learning for deep Gaussian process
526 surrogates. *arXiv:2012.08015*.
- 527 Stein, M. L. (1999). *Interpolation of Spatial Data: Some Theory for Kriging*. Springer, New
528 York.
- 529 Tripathy, R., Bilonis, I., and Gonzalez, M. (2016). Gaussian processes with built-in dimen-
530 sionality reduction: applications to high-dimensional uncertainty propagation. *Journal of*
531 *Computational Physics*, 321:191–223.
- 532 Vernon, I., Jackson, S. E., and Cumming, J. A. (2019). Known boundary emulation of complex
533 computer models. *SIAM/ASA Journal on Uncertainty Quantification*, 7(3):838–876.
- 534 Watson-Parris, D. (2021). Machine learning for weather and climate are worlds apart. *Philo-*
535 *sophical Transactions of the Royal Society A*, 379(2194):20200098.